

DISCOVERY AND IDENTIFICATION OF  
EXTRA GAUGE BOSONS <sup>1</sup>

Mirjam Cvetič

*Department of Physics, University of Pennsylvania  
Philadelphia, PA 19104-6396*

and

Stephen Godfrey

*Department of Physics, Carleton University  
Ottawa, ON K1S 5B6***Abstract**

The discovery potential and diagnostic abilities of proposed future colliders for new heavy neutral ( $Z'$ ) and charged ( $W'$ ) gauge bosons are summarized. Typical bounds achievable on  $M_{Z',W'}$  at the TEVATRON, DTEVATRON, LHC, 500 GeV NLC, and 1 TeV NLC are  $\sim 1$  TeV,  $\sim 2$  TeV,  $\sim 4$  TeV, 1–3 TeV, and 2–6 TeV, respectively. For  $M_{Z'} \sim 1$  TeV the LHC will have the capability to determine the magnitude of normalized  $Z'$  quark and lepton couplings to around 10–20%, while the NLC would allow for determination of the couplings (including their signs) with a factor of 2 larger error-bars, provided heavy flavor tagging and longitudinal polarization of the electron beam is available.

**1 Introduction**

The existence of heavy neutral ( $Z'$ ) and/or charged ( $W'$ ) vector bosons are a feature of many extensions of the standard model (SM). They arise in extended gauge theories including grand unified theories [1], superstring theories [2], and Left-Right symmetric models [3] and in other models such as the BESS model [4] and models of composite gauge bosons [5].

In this report we survey and compare the discovery potential of the experiments that will be performed over the next decade (TEVATRON, HERA, and

---

<sup>1</sup>Summary of the Working Subgroup on Extra Gauge Bosons of the DPF long-range planning study to be published in *Electro-weak Symmetry Breaking and Beyond the Standard Model*, eds T. Barklow, S. Dawson, H. Haber and J. Seigrist (World Scientific 1995).

LEP200) and future facilities that are being planned and considered for the period beyond (various TEVATRON upgrades, the LHC  $pp$  collider, the LSGNA 60 TeV  $pp$  collider, the NLC  $e^+e^-$  collider, and the LEP-LHC  $ep$  collider). In addition to the discovery reach of each of the experimental facilities we also address the auxiliary question; that of the measurement of the properties of a newly discovered gauge boson and therefore its identification in the context of a specific model. We therefore examine the diagnostic power of future colliders for heavy gauge boson physics, in particular, a (model independent) determination of heavy gauge boson couplings to quarks and leptons.

In the next Section we give a brief description of the various models with new gauge bosons that will be used in the study. Given that models without gauge invariance will most likely reveal themselves in ways other than the discovery of extra gauge bosons, we will restrict our analysis to heavy gauge bosons that arise in models with extended gauge symmetries. In Section 3 we summarize current constraints on heavy gauge bosons. In Section 4 we describe the signatures of extra gauge bosons at future hadron and  $e^+e^-$  colliders and the resulting discovery reaches. In Section 5 we address the diagnostic power (identification potential) for heavy gauge boson physics at the LHC and the NLC, respectively. Conclusions are given in Section 6.

There is a large and growing literature on this subject of which we address only some aspects. Our primary goal is to explore the potential of experimental facilities for extra gauge bosons physics over the next decade and beyond. The emphasis is on comparing the discovery limits as well as the diagnostic power of the different facilities. Other useful reviews which address related topics, some of them in more detail, are: Hewett and Rizzo [6], Hewett [7], Cvetič, del Aguila and Langacker [8], and del Aguila [9].

## 2 Models of Extra Gauge Bosons

In this section we briefly describe some of the extended gauge theories which have been studied in the literature. While not totally comprehensive, the properties are representative of models with extra gauge bosons.

### 2.1 Effective Rank-5 Models

The largest set of extended gauge theories are those which are based on GUTS [6]. Popular examples are the groups  $SO(10)$  and  $E_6$ . Generically, additional  $Z$ -bosons originating from  $E_6$  grand unified theories are conveniently labeled in terms of the chain

$$E_6 \rightarrow SO(10) \times U(1)_\psi \rightarrow SU(5) \times U(1)_\chi \times U(1)_\psi \rightarrow SM \times U(1)_{\theta_{E_6}} \quad (1)$$

where  $U(1)_{\theta_{E_6}}$  remains unbroken at low energies. Thus, the  $Z'$  charges are given by linear combinations of the  $U(1)_\chi$  and  $U(1)_\psi$  charges resulting in the  $Z'$ -fermion couplings:

$$g_{Z^0} \left( \frac{g_{Z'}}{g_{Z^0}} \right) (Q_\chi \cos \theta_{E_6} + Q_\psi \sin \theta_{E_6}) \quad (2)$$

where  $\theta_{E_6}$  is a free parameter which lies in the range  $-90^\circ \leq \theta_{E_6} \leq 90^\circ$ ,  $(g_{Z'}/g_{Z^0})^2 \leq \frac{5}{3} \sin^2 \theta_w$  (here we assume the equality),  $Q_\psi = [1, 1, 1]/2\sqrt{6}$ , and  $Q_\chi = [-1, 3, -5]/2\sqrt{10}$  for  $[(u, d, u^c, e^c), (d^c, \nu e^-), (N^c)]$ , the left-handed fermions in the **10**,  $\bar{\mathbf{5}}$ , and **1** of  $SU(5)$  contained in the usual **16** of  $SO(10)$ . Special cases of interest are model  $\chi$  ( $\theta_{E_6} = 0^\circ$ ) corresponding to the extra  $Z'$  of  $SO(10)$ , model  $\psi$  ( $\theta_{E_6} = 90^\circ$ ) corresponding to the extra  $Z'$  of  $E_6$ , and model  $\eta$  ( $\theta_{E_6} = \arctan -\sqrt{5/3}$ ) corresponding to the extra  $Z'$  arising in some superstring theories [2].

## 2.2 Left-Right Symmetric Model (LRM)

$SO(10)$  GUTS lead to intermediate symmetries, for example;

$$\begin{aligned} SO(10) &\rightarrow SU(3)_C \times SU(2)_L \times U(1)_Y \times U(1)_\chi \\ &\rightarrow SU(3)_C \times SU(2)_L \times SU(2)_R \times U(1)_{B-L} \end{aligned} \quad (3)$$

The first chain leads to the additional  $Z$ -boson,  $Z_\chi$ , mentioned above, while the second chain yields the left-right symmetric model (LRM) which extends the standard model gauge group to  $SU(2)_L \times SU(2)_R \times U(1)$  [3] with a right-handed charged boson as well as an additional neutral current. The  $Z'$ -fermion coupling is given by

$$g_{Z^0} \frac{1}{\sqrt{\kappa - (1 + \kappa)x_W}} [x_W T_{3L} + \kappa(1 - x_W) T_{3R} - x_W Q] \quad (4)$$

with  $0.55 \leq \kappa^2 \equiv (g_R/g_L)^2 \leq 1 - 2$  [10],  $T_{3L(R)}$  the isospin assignments of the fermions under  $SU(2)_{L(R)}$ ,  $Q$  the fermion electric charge and  $x_W = \sin \theta_W$ . We assume  $\kappa = 1$  in our analysis which corresponds to manifest left-right symmetric gauge interactions. Note that the  $T_{3L}$  assignments are the same as in the standard model while the values of  $T_{3R}$  for  $u_R, d_R, e_R, \nu_R = \frac{1}{2}, -\frac{1}{2}, -\frac{1}{2}, \frac{1}{2}$  and are zero for left-handed doublets.

## 2.3 Alternative Left-Right Symmetric Model (ALRM)

Another extended model based on the second intermediate group is the alternative left-right model (ALRM) which originates from  $E_6$  GUT's and is also based on the electroweak gauge group  $SU(2)_L \times SU(2)_R \times U(1)$  [11]. Here the assignments for  $T_{3L(R)}$  differ from those of the usual LRM for  $\nu_{L,R}, e_L$ , and  $d_R$  with  $T_{3L(R)}(\nu_L) = \frac{1}{2}(-\frac{1}{2})$ ,  $T_{3L(R)}(e_L) = -\frac{1}{2}(-\frac{1}{2})$ , and  $T_{3L(R)}(d_R) = 0$ . The LRM and ALRM have

identical  $u$ -quark,  $e_R$ , and  $d_L$  couplings. In this model the right handed  $W$ -boson carries lepton number and has odd R-parity avoiding the usual constraints on the mass of right handed  $W$ 's.

## 2.4 “Sequential” Standard Model (SSM)

The “sequential” Standard Model (SSM) consists of a  $Z'$  with the same couplings as the SM  $Z^0$  boson couplings. Although it is not a gauge invariant model it is often used for purposes of comparison.

## 2.5 Un-unified Standard Model (UNSM)

The un-unified standard model (UNSM) [12] is based on the gauge group  $SU(2)_l \times SU(2)_q \times U(1)_Y$ , i.e., left-handed leptons (quarks) transform as doublets under  $SU(2)_l$  ( $SU(2)_q$ ) and singlets under  $SU(2)_q$  ( $SU(2)_l$ ), and right-handed fields are singlets under both groups. The  $Z'$ -fermion coupling takes the form

$$g_{Z^0} c_w \left( \frac{T_{3q}}{\tan \phi} - \tan \phi T_{3l} \right) \quad (5)$$

where  $T_{3q(l)}$  is the third component of  $SU(2)_{q(l)}$ -isospin,  $c_w = \cos \theta_w$ , and  $\phi$  is a mixing parameter which lies in the range  $0.22 \leq \sin \phi \leq 0.99$ . We take  $\sin \phi = 0.5$  in our calculations. The  $Z'$  is purely left handed in this model.

There are numerous other models predicting  $Z'$ 's in the literature [13] but the subset described above has properties representative of the broad class of models, at least for the purposes of comparing discovery limits at high energy colliders.

In all of the above models the  $Z - Z'$  mass matrix takes the form

$$M^2 = \begin{pmatrix} M_Z^2 & \gamma M_Z^2 \\ \gamma M_Z^2 & M_{Z'}^2 \end{pmatrix} \quad (6)$$

where  $\gamma$  is determined within each model once the Higgs sector is specified. The physical eigenstates are then

$$\begin{aligned} Z_1 &= Z' \sin \phi + Z \cos \phi \\ Z_2 &= Z' \cos \phi - Z \sin \phi \end{aligned} \quad (7)$$

where  $Z_1$  is currently being probed at LEP and  $\tan 2\phi = 2\gamma M_Z^2 / (M_Z^2 - M_{Z'}^2)$ . LEP measurements constrain  $|\phi| < 0.01$  [14] which is smaller than could be observed at high energy collider experiments. Without loss of generality we will therefore ignore  $Z - Z'$  mixing in the remainder of this review.

In this report we will also assume that the branching ratios include decays into only *three ordinary families*.

### 3 Present Limits

Before proceeding to future colliders it is useful to list existing bounds as a benchmark against which to measure future experiments. Constraints can be placed on the existence of  $Z'$ 's either indirectly from fits to high precision electroweak data [14]–[17] or from direct searches at operating collider facilities [18].

There have been a number of fits to precision data [14, 15]. We list results<sup>2</sup> of Langacker [16] in Table 1 which includes the most recent (1993) LEP data and is an update of the global analysis of electro-weak data described in Ref. [14]. Two sets of results are presented; an unconstrained fit with no assumptions on the Higgs sector, and a constrained fit with specific assumptions on the Higgs sector and therefore the  $Z^0 - Z'$  mixing angle.

The highest mass limits come from direct searches by the CDF experiment at the Tevatron [18]. The CDF limits are obtained by looking for high invariant mass lepton pairs that would result from Drell-Yan production of  $Z'$ 's and  $W'$ 's [20, 21] and their subsequent decay to lepton pairs;  $p\bar{p} \rightarrow Z' \rightarrow \ell^+\ell^-$  and  $p\bar{p} \rightarrow W' \rightarrow \ell^\pm \not{p}_T$ . The most recent CDF 95 % confidence level results based on  $\mathcal{L}_{int} = 19.6\text{pb}^{-1}$  are listed in Table 1. The next run with  $\sim 75\text{pb}^{-1}$  will increase the discovery reach by roughly 100 GeV.

The direct TEVATRON bounds on  $M_{W'_{LR}}$  (for the main production channel  $pp \rightarrow W' \rightarrow e\nu_e$ ) are in the 600 GeV region, while indirect constrained [unconstrained] bounds are in the 1.4 TeV [300 GeV] region.

Table 1: Current constraints on  $M_{Z'}$  (in GeV) for typical models from direct production at the TEVATRON ( $\mathcal{L}_{int} = 19.6\text{pb}^{-1}$ ), as well as indirect limits from a global electro-weak analysis (95% C.L.) [16].

	direct	indirect (unconstrained)	indirect (constrained)
$\chi$	425	330	920
$\psi$	415	170	170
$\eta$	440	220	610
$LR$	445	390	1360
$SSM$	505	960	

---

<sup>2</sup>The analysis for current limits on extra gauge bosons in the un-unified standard model (UNSM) was done in Ref. [19].

## 4 Discovery Limits of Extra Gauge Bosons

In this section we present the discovery reach for some of the models which exist in the literature, and were described in Section 2. Although far from exhaustive, these models form a representative set for the purposes of comparison.

Bounds on extra gauge bosons attainable from low energy neutral current precision experiments, measurements at the TRISTAN, LEP and SLC  $e^+e^-$  colliders, as well as at the HERA  $ep$  collider have been surpassed by direct limits obtained at the TEVATRON  $p\bar{p}$  collider or will be from planned TEVATRON upgrades [22, 23]. We will therefore restrict the analysis to LEP200, proposed TEVATRON upgrades, the LHC- $pp$  collider, the LSGNA 60 TeV  $pp$  collider, the NLC-high luminosity  $e^+e^-$  collider, and the LEP-LHC  $ep$  collider [22, 23, 24].

### 4.1 Hadron Colliders

The signal for a  $Z'$  at a hadron collider consists of Drell-Yan production of lepton pairs [1, 21, 22, 23, 25] with high invariant mass via  $p \bar{p} \rightarrow Z' \rightarrow l^+l^-$ . The cross section for the production of on-shell  $Z'$ s is given by [22]:

$$\frac{d\sigma(pp \rightarrow f\bar{f})}{dy} = \frac{x_A x_B \pi^2 \alpha_{em}^2 (g_{Z'}/g_{Z^0})^4}{9M_{Z'}\Gamma_{Z'}} \left( C_L^{f^2} + C_R^{f^2} \right) \sum_q \left( C_L^{q^2} + C_R^{q^2} \right) G_q^+(x_A, x_B, Q^2) \quad (8)$$

where

$$G_q^+(x_A, x_B, Q^2) = \sum_q \left[ f_{q/A}(x_A) f_{\bar{q}/B}(x_B) + f_{\bar{q}/A}(x_A) f_{q/B}(x_B) \right] \quad (9)$$

The cross section for  $Z'$  production at hadron colliders is inversely proportional to the  $Z'$  width. If exotic decay modes are kinematically allowed, the  $Z'$  width will become larger and more significantly the branching ratios to conventional fermions smaller. This is not important in  $e^+e^-$  and  $ep$  collisions since those processes proceed via virtual  $Z'$ s in contrast to hadron colliders which rely on the Drell-Yan production of real  $Z'$ s. Having said this we will only consider the case that no new decay modes are allowed. The partial widths are given (at tree level) by

$$\Gamma_{Z' \rightarrow f\bar{f}} = M_{Z'} g_{Z'}^2 (C_{f_L}^2 + C_{f_R}^2) / 24\pi \quad (10)$$

The cross section for  $\sigma(pp \rightarrow Z') \cdot \text{BR}(Z' \rightarrow \ell^+\ell^-)$  is shown in Fig. 1 as a function of  $M_{Z'}$  for an upgraded Tevatron ( $p\bar{p}$ ) with  $\sqrt{s} = 4$  TeV and the LHC ( $pp$ ) with  $\sqrt{s} = 14$  TeV. If we use 10 dilepton events clustered at a particular invariant mass as the criteria for discovery of a  $Z'$  one can read off the discovery reach as the cross section times integrated luminosity which gives this number of dilepton events.

We obtain the discovery limits for this process based on 10 events in the  $e^+e^- + \mu^+\mu^-$  channels using the EHLQ structure functions [25] set 1, taking  $\alpha = 1/128.5$ ,

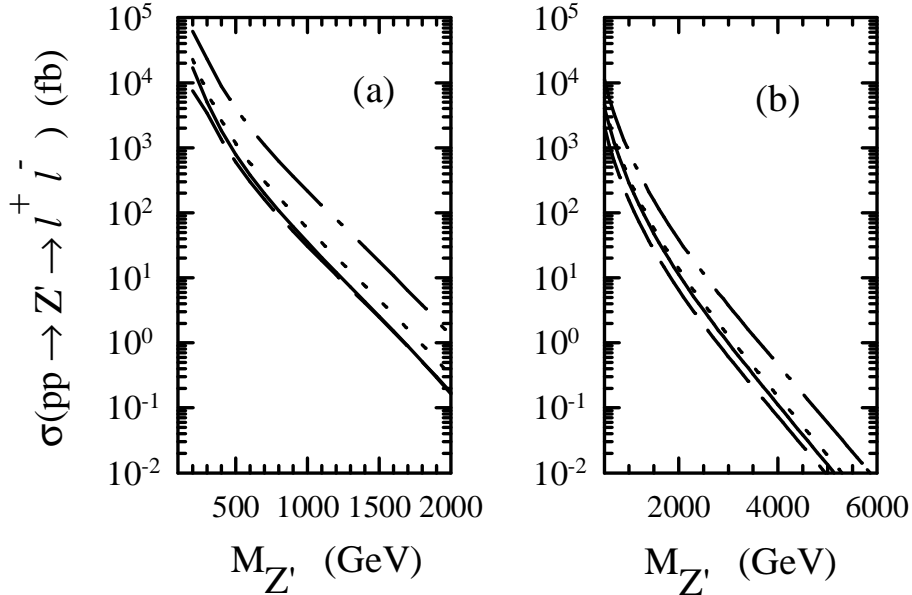


Figure 1: The cross section for the process  $pp \rightarrow Z' \rightarrow \ell^+\ell^-$  as a function of  $M_{Z'}$  for (a)  $p\bar{p}$  with  $\sqrt{s} = 4$  TeV and (b)  $pp$  with  $\sqrt{s} = 14$  TeV. In both cases the solid line is for  $Z_\chi$ , the dashed line for  $Z_\psi$ , the dotted line for  $Z_{LR}$  and the dot-dashed line for  $Z_{ALR}$ .

$\sin^2\theta_w = 0.23$ , and including a 1-loop  $K$ -factor in the  $Z'$  production [26]. We include a  $t$ -quark of mass 174 GeV in the  $Z'$  decay width, and 2-loop QCD radiative corrections and 1-loop QED radiative corrections in calculating the  $Z'$  width. Using different quark distribution functions results in a roughly 10% variation in the  $Z'$  cross sections [27] with the subsequent change in discovery limits. We note that including realistic detector efficiencies would lower these limits.

Lowering the number of events in the  $e^+e^- + \mu^+\mu^-$  channels to 6 raises the discovery reach about 10% while lowering the luminosity by a factor of ten reduces the reach by about a factor of 3 [22].

In our calculations we assumed that the  $Z'$  only decays into the three conventional fermion families. If other decay channels were possible, such as to exotic fermions filling out larger fermion representations or supersymmetric partners, the  $Z'$  width would be larger, lowering the discovery limits. On the other hand, if decays to exotic fermions were kinematically allowed, the discovery of exotic fermions would be an important discovery in itself; the study of the corresponding decay modes would provide additional information on the nature of the extended gauge structure.

The discovery limits for various models at hadron colliders are listed in Table 2 and, for ease of comparison, are shown in Fig. 3 along with those of  $e^+e^-$  colliders, both given at the end of this section. These bounds are relatively insensitive to specific models. In addition, since they are based on a distinct signal with little background they are relatively robust limits. For the case of the DI-TEVATRON ( $\sqrt{s} = 4$  TeV), the  $p\bar{p}$  option has a 50% higher discovery reach than the  $pp$  option for a given luminosity indicating that valence quark contributions to the Drell-Yan production process are still important at these energies.

Discovery limits for  $W'$  bosons obtained using the process  $pp$  ( $p\bar{p}$ )  $\rightarrow W'^{\pm} \rightarrow \ell^{\pm}\nu_{\ell}$  and are based on 10 events in the  $[(e^+\nu_e + e^-\bar{\nu}_e) + (\mu^+\nu_{\mu} + \mu^-\bar{\nu}_{\mu})]$  channels. They are given in Table 2. The  $W'$  discovery limits are larger than the comparable  $Z'$  limits which is in part due to the fact that in most models with  $W'$ 's [*e.g.*, the left-right symmetric model(s)] the  $W'$  couplings are comparable in magnitude with those of the standard model  $W$ . These results are based [28] on conservative assumptions on the form of the CKM matrix, *i.e.*, the right-handed and left-handed quark-mixing matrix elements have an equal magnitude. If these assumptions are relaxed [28, 29], the bounds could change drastically.

## 4.2 $e^+e^-$ Colliders

At  $e^+e^-$  colliders discovery limits are indirect, being inferred from deviations from the standard model predictions for various cross sections and asymmetries due to interference between the  $Z'$  propagator and the  $\gamma$  and  $Z^0$  propagators [30]. This effect is similar to PEP/PETRA seeing the standard model  $Z^0$  as deviations from the predictions of QED. The basic process is  $e^+e^- \rightarrow f\bar{f}$  where  $f$  could be leptons ( $e, \mu, \tau$ ) or quarks ( $u, d, c, s, b$ ). For  $e^+e^-$  collider measurements all results are derived from the differential cross section for a polarized  $e^-$  and an unpolarized  $e^+$  [22]:

$$\frac{d\sigma(e^+e^- \rightarrow f\bar{f})}{d\cos\theta} = \frac{\pi\alpha^2}{4s} \left\{ |C_{LL}|^2(1 + \cos\theta)^2 + |C_{LR}|^2(1 - \cos\theta)^2 \right\} \quad (11)$$

where

$$C_{ij} = -Q_f + \frac{C_i^e C_j^f}{\sin^2\theta_W \cos^2\theta_W} \left( \frac{s}{s - M_{Z^0}^2 + i\Gamma_{Z^0} M_{Z^0}} \right) + \frac{(g_{Z'}/g_{Z^0})^2 C_i^{e'} C_j^{f'}}{\sin^2\theta_W \cos^2\theta_W} \left( \frac{s}{s - M_{Z'}^2 + i\Gamma_{Z'} M_{Z'}} \right) \quad (12)$$

From these basic reactions the following probes are used to search for the effects of  $Z'$ 's:

- The leptonic cross section,  $\sigma(e^+e^- \rightarrow \mu^+\mu^-)$ .



- The ratio of the hadronic to the QED point cross section,  $R^{had} = \sigma^{had}/\sigma_0$ .
- The leptonic forward-backward asymmetry,  $A_{FB}^\ell$ , and if  $c$  and  $b$  quark flavor tagging were sufficiently efficient, one could measure  $A_{FB}(e^+e^- \rightarrow c\bar{c})$  and  $A_{FB}(e^+e^- \rightarrow b\bar{b})$ . The forward-backward asymmetries are given by:

$$A_{FB} = \frac{[\int_0^1 - \int_{-1}^0] d \cos \theta \frac{d\sigma}{d \cos \theta}}{[\int_0^1 + \int_{-1}^0] d \cos \theta \frac{d\sigma}{d \cos \theta}} \quad (13)$$

- The leptonic longitudinal asymmetry,  $A_{LR}^\ell$ , the hadronic longitudinal asymmetry,  $A_{LR}^{had} = A_{LR}(e^+e^- \rightarrow hadrons)$ , and final state polarization of  $\tau$ 's,  $A_{pol}^\tau$ . These polarization asymmetries are defined by

$$A_{LR} = \frac{\sigma(e_L^-) - \sigma(e_R^-)}{\sigma(e_L^-) + \sigma(e_R^-)} \quad (14)$$

where the cross sections are obtained by integrating eq. 4.4 over  $\cos \theta$ . (For electron polarization less than 100% the asymmetry is given by  $A_{LR}^P = PA_{LR}^{P=1}$ .) Since the cross section to hadrons is much larger than to leptons this results in higher statistics and therefore more precise measurements.

- The polarized forward-backward asymmetry for specific fermion flavors,  $A_{FB}^f(pol)$  is obtained by considering the forward-backward asymmetry for specific initial electron polarizations.

In these expressions the indices  $f = \ell$ ,  $q$ ,  $\ell = (e, \mu, \tau)$ ,  $q = (c, b)$ , and  $had =$ 'sum over all hadrons' indicate the final state fermions.

For indirect limits, a 99% C.L. corresponds to a  $2\sigma$  effect of one observable. Since  $2\sigma$  deviations are not uncommon one must be cautious about how one obtains discovery limits for  $Z'$ 's. One possibility for obtaining believable limits is to raise the deviation required to indicate the existence of a  $Z'$ . A second possibility is to combine several observables to obtain a  $\chi^2$  figure of merit. We follow the second approach here by including  $\sigma^l$ ,  $R^{had}$ ,  $A_{LR}$ , and  $A_{LR}^{had}$  to obtain the 99% confidence limits. In Fig. 2 we show these observables for representative models as a function of  $M_{Z'}$ .  $1-\sigma$  statistical errors are shown for comparison with the deviations resulting from the existence of a  $Z'$ . The discovery limits obtained this way are given in Table 2 and shown in Fig. 3 at the end of this section.<sup>3</sup>

One sees that the discovery limits obtained at  $e^+e^-$  colliders are as high or higher than those that can be obtained at hadron colliders. However, the bounds obtained are more model dependent than the bounds obtained at hadron colliders.

---

<sup>3</sup>Although it is far from clear whether LEP200 will achieve any significant longitudinal polarization,  $A_{LR}^{had}$  only contributes significantly to the limit on  $Z_\chi$  at LEP200 so that our results are not in general sensitive to the inclusion of this observable in the  $\chi^2$  at LEP200.

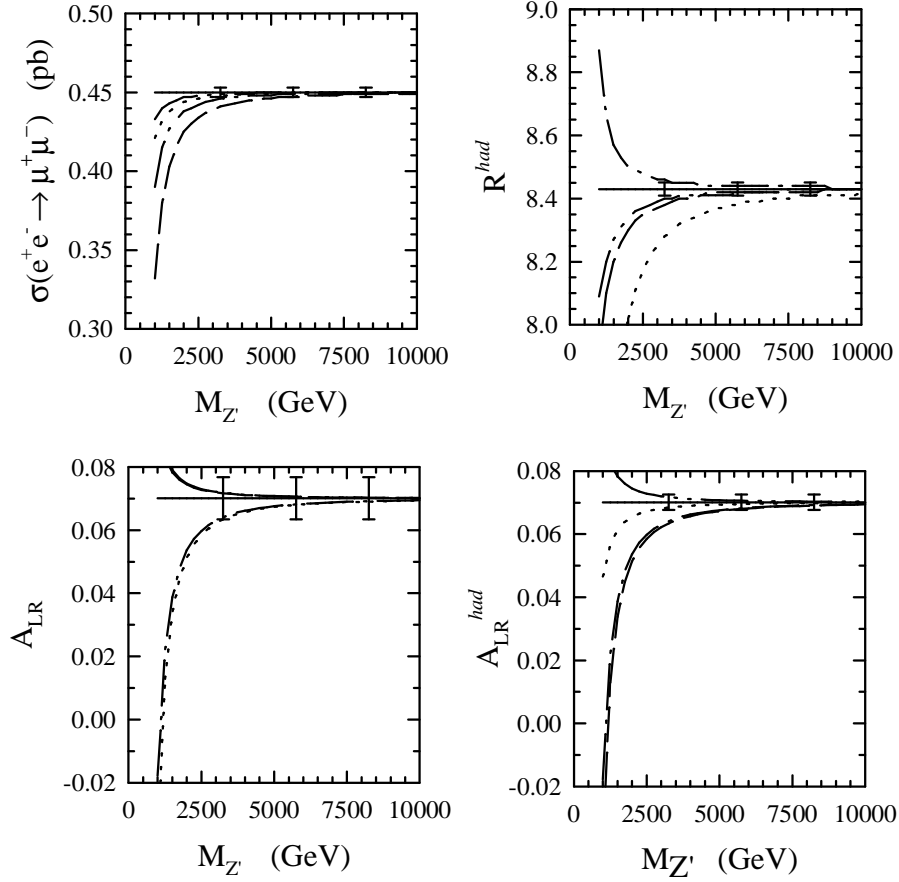


Figure 2:  $\sigma(e^+e^- \rightarrow \mu^+\mu^-)$ ,  $R_{had}$ ,  $A_{LR}$ , and  $A_{LR}^{had}$  for  $\sqrt{s} = 500$  GeV as a function of  $M_{Z'}$ . The error bars are statistical errors based on  $50 \text{ fb}^{-1}$  integrated luminosity. In all cases the solid line is the standard model prediction, the dot-dash line is for model- $\chi$ , the dot-dot-dash model is for model-LR, the dashed line is for model-ALR and the dotted line is for model-SSM.

For example, for model  $\psi$ ,  $C'_L = \pm C'_R$  so that either  $C'_V$  or  $C'_A = 0$ . For  $\sqrt{s}$  sufficiently far away from the  $Z^0$  pole deviations are dominated by  $Z^0 - Z'$  and  $\gamma - Z'$  interference which is proportional to  $C_V^2 C_V'^2 + 2C_V C_A C_V' C_A' + C_A^2 C_A'^2$ . Since for the photon  $C_A = 0$  so when  $C'_V$  is also equal to 0, deviations from the standard model become small.

Because the bounds obtained at  $e^+e^-$  colliders are indirect, based on deviations from the standard model in precision measurements, they are sensitive to the experimental errors, both statistical and systematic. For example, reducing the LEP200 integrated luminosity from 500 pb<sup>-1</sup> to 250 pb<sup>-1</sup> reduces the discovery limits by about 15% and reducing the NLC integrated luminosity from 50 fb<sup>-1</sup> to 10 fb<sup>-1</sup> (200 fb<sup>-1</sup> to 50 fb<sup>-1</sup>) for the 500 GeV (1 TeV) case reduces the discovery limit by about 33%. Including a 5% systematic error in cross section measurements and a 2% systematic errors in asymmetries where systematic errors partially cancel [31] can lower the discovery limits significantly. The most extreme change is for the sequential standard model  $Z'$  which decreases by a factor of 2 at LEP200 and a factor of 3 at the NLC. Clearly, systematic errors will have to be kept under control for high precision measurements.

We did not include radiative corrections in our results. In general, this is an acceptable procedure since we are looking for small deviations from the standard model predictions and radiative corrections to  $Z'$  contributions will be a small correction to a small effect. However, QED bremsstrahlung corrections, in particular initial state radiation, can give large contributions to the observables, altering the statistics we assumed. Since these are dependent on details of the detector we have left them out, but note that they can alter the numerical values.

### 4.3 $ep$ Colliders

A final type of collider that exists and is being considered for the future are  $ep$  colliders; HERA at DESY and LEP-LHC and LEP2-LHC at CERN [32, 33]. As in the  $e^+e^-$  case  $Z'$  discovery is based on deviations from the standard model for high precision measurements of various observables. The diagrams are similar to those of the hadron-collider and  $e^+e^-$  cases except that the gauge bosons are exchanged in the  $t$ -channel in contrast to  $s$ -channel production in the former cases. The differential cross section for  $ep$  collisions is given by:

$$\frac{d\sigma(e^-p)}{dx dy} = \frac{2\pi\alpha^2}{s x^2 y^2} \sum_q \left\{ x f_q(x, Q^2) [ |b_{LL}|^2 + |b_{LR}|^2 (1-y)^2 ] \right. \\ \left. + x f_{\bar{q}}(x, Q^2) [ |b_{LR}|^2 + |b_{LL}|^2 (1-y)^2 ] \right\} \quad (15)$$

where the sum runs over quark flavors.  $f_q(x, Q^2)$  and  $f_{\bar{q}}(x, Q^2)$  are the quark and antiquark distribution functions,  $Q^2 = xys = -q^2$ , and  $x$  and  $y$  are the usual

scaling variables,  $x = Q^2/2p \cdot q$ ,  $y = p \cdot q/p \cdot k$ . The functions  $b_{ij}$  are given by

$$b_{ij} = -Q_q + \frac{C_i^e C_j^q}{\sin^2 \theta_W \cos^2 \theta_W} \frac{Q^2}{Q^2 + M_{Z^0}^2} + \left( \frac{g_{Z'}}{g_{Z^0}} \right)^2 \frac{C_i^{e'} C_j^{q'}}{\sin^2 \theta_W \cos^2 \theta_W} \frac{Q^2}{Q^2 + M_{Z'}^2} \quad (16)$$

where  $Q_q$  denotes the quark electric charge and  $C_{L,R}$  and  $C'_{L,R}$  are the left and right-handed  $Z^0$  and  $Z'$  charges. For the  $e_L^+ p$  cross section take  $b_{LL} \rightarrow b_{RL}$  and  $b_{LR} \rightarrow b_{RR}$  and to obtain the cross section for right-handed electrons and positrons make the substitution  $L \leftrightarrow R$ .

Given longitudinal polarization of incident  $e^-$  or  $e^+$  there are eight different measurements (of which four are independent); the electron and positron cross sections  $\sigma(e^-)$  and  $\sigma(e^+)$ , and the six asymmetries  $e_L^- - e_R^-$ ,  $e_L^- - e_R^+$ ,  $e_R^- - e_L^+$ ,  $e_L^+ - e_R^+$ ,  $e_R^- - e_R^+$ , and  $e_L^- - e_L^+$  where the asymmetry  $\alpha - \beta$  is defined as

$$A_{\alpha\beta} = \frac{\sigma(\alpha) - \sigma(\beta)}{\sigma(\alpha) + \sigma(\beta)}. \quad (17)$$

To obtain discovery limits based on deviations from the standard model we follow the same approach used in obtaining limits at  $e^+e^-$  colliders. We base our limits using a  $\chi^2$  analysis of the four observables;  $A(e_L^- - e_R^-)$ ,  $A(e_L^- - e_R^+)$ ,  $A(e_R^- - e_L^+)$ , and  $A(e_L^+ - e_R^+)$ . Unlike the  $e^+e^-$  analysis the deviations vary significantly for the different observables [22, 32] and the  $\chi^2$  tends to be dominated by only one or two of them.

We used the EHLQ structure functions [25] (set 2), integrated over the  $x$  and  $y$  variables from 0.1 to 1. The lower bound was so chosen because at small  $x$  the cross section is larger giving better statistics, but with smaller deviations, while at large  $x$  the deviations are larger, but the statistics are poorer. Thus, we take  $x_{min} = 0.1$  as a reasonable compromise with adequate statistics which is not overwhelmed by the standard model contributions. More sophisticated event binning would likely improve our bounds.

The results for the various  $ep$  options are given in Table 2. Despite the fact that for HERA we used the overly optimistic integrated luminosity of  $600 \text{ pb}^{-1}$  per polarization the discovery limits for HERA have already been surpassed by existing Tevatron results. Similarly, the discovery limits at the LEP-LHC  $ep$  collider are not at all competitive with the LHC and are at the verge of being excluded by the TEVATRON. The higher energy, but lower luminosity LEP2-LHC option are essentially irrelevant. Even if LEP2-LHC could achieve integrated luminosities of  $1 \text{ fb}^{-1}$  the discovery limits would only yield a small improvement over the bounds achievable at (the lower energy) LEP-LHC option.

Table 2: Bounds on  $M_{Z'}$  and  $M_{W'_{LR}}$  (in GeV) for typical models achievable at proposed hadron and  $e^+e^-$  colliders. The discovery limits for  $Z'$  [ $W'^++W'^-$ ] at hadron colliders are for typical models with 10 events in  $e^+e^- + \mu^+\mu^- [(e^+\nu_e+e^-\bar{\nu}_e) + (\mu^+\nu_\mu+\mu^-\bar{\nu}_\mu)]$  while those for  $e^+e^-$  colliders are 99% C.L. obtained from a  $\chi^2$  based on  $\sigma(e^+e^- \rightarrow \mu^+\mu^-)$ ,  $R^{had} = \sigma(e^+e^- \rightarrow hadrons)/\sigma_0$ ,  $A_{LR}^{\mu^+\mu^-}$ , and  $A_{LR}^{had}$ .

Collider	$\sqrt{s}$ [TeV]	$\mathcal{L}_{int}$ [fb $^{-1}$ ]	$\chi$	$\psi$	$\eta$	$LR$	$W'_{LR}$
TEVATRON ( $p\bar{p}$ )	1.8	1	775	775	795	825	920
TEVATRON' ( $p\bar{p}$ )	2	10	1040	1050	1070	1100	1180
DI-TEVATRON ( $p\bar{p}$ )	4	20	1930	1940	1990	2040	2225
LHC ( $pp$ )	10	40	3040	2910	2980	3150	
LHC ( $pp$ )	14	100	4380	4190	4290	4530	5310
LEP200 ( $e^+e^-$ )	0.2	0.5	695	269	431	493	
NLC ( $e^+e^-$ )	0.5	50	3340	978	1990	2560	
NLC-A ( $e^+e^-$ )	1.0	200	6670	1940	3980	5090	
NLC-B ( $e^+e^-$ )	1.5	200	8220	2550	4970	6240	
NLC-C ( $e^+e^-$ )	2.0	200	9560	3150	5830	7210	
HERA ( $ep$ )	0.314	0.6	235	125	215	495	
LEP $\times$ LHC ( $ep$ )	1.183	1.0	375	—	435	1060	
LEP2 $\times$ LHC ( $ep$ )	1.670	0.1	—	—	—	615	

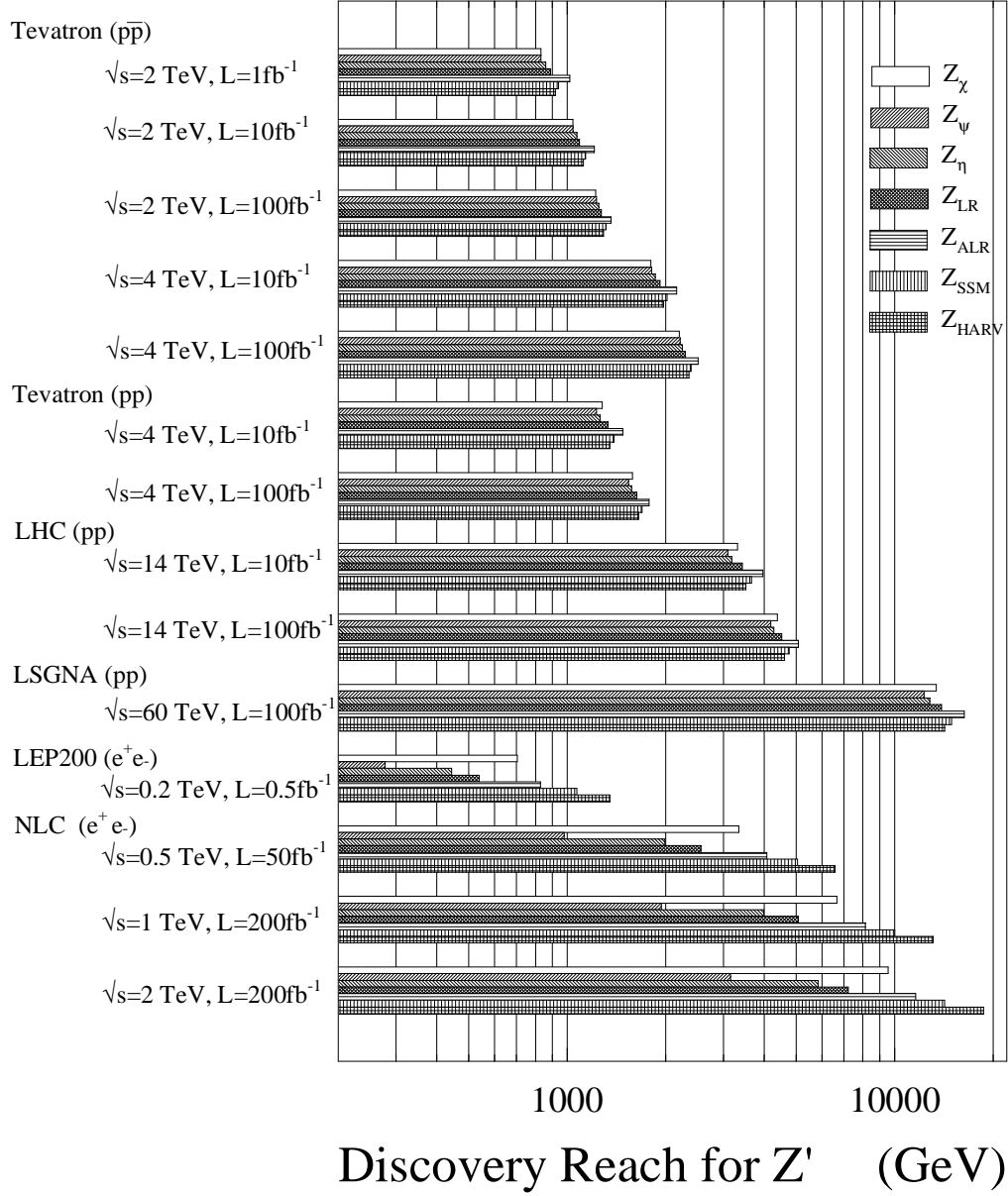


Figure 3: Discovery limits for extra neutral gauge bosons ( $Z'$ ) for the models described in the text. The discovery limits at hadron colliders are based on 10 events in the  $e^+e^- + \mu^+\mu^-$  channels while those for  $e^+e^-$  colliders are 99% C.L. obtained from a  $\chi^2$  based on  $\sigma(e^+e^- \rightarrow \mu^+\mu^-)$ ,  $R^{had} = \sigma(e^+e^- \rightarrow hadrons)/\sigma_0$ ,  $A_{LR}^{\mu^+\mu^-}$ , and  $A_{LR}^{had}$ . The integrated luminosities are based on a  $10^7$  sec year of running.

## 5 New Gauge Boson Diagnostics at Future Colliders (LHC & NLC)

An immediate need after the discovery of a new gauge boson would be to determine its origin by measuring its properties [34]:

1.  $Z'$  couplings to quarks and leptons.
2. The nature of the symmetry breaking sector.
3.  $Z'$  couplings to exotics.

A test of the symmetry breaking structures are the decays  $Z' \rightarrow W^+W^-$  [35, 36], which are suppressed by  $Z - Z'$  mixing but still have a sizable rate due to the enhancement of the longitudinal components of the  $W$  bosons. However, they suffer from serious QCD backgrounds [37, 38]. In theories with charged gauge bosons, *e.g.*, left-right (LR) symmetric models, the ratio  $M_{Z'}/M_{W'}$  plays an analogous role to the  $M_Z/M_W$  ratio (related to the  $\rho$  parameter) in the standard model. This ratio therefore yields indirect information on the nature of the Higgs sector [39].

The study of  $Z'$  decays into exotic particles also yields useful information. In particular,  $W' \rightarrow \ell N$  and  $Z' \rightarrow NN$  and subsequent decays of heavy right-handed neutrinos  $N$  turn out to be useful probes for distinguishing the left-right models from those with only an additional  $U(1)$  [36, 40].

In the following we will concentrate on the diagnostic study of new gauge boson couplings to quarks and leptons. In Subsection 5.1 we address the new gauge boson diagnostics at the LHC. In Subsection 5.2 we present an analogous analysis at the NLC. The comparison of the diagnostic power of the two types of machines is given in Subsection 5.3.

### 5.1 New Gauge Boson Diagnostics at the LHC

In the main production channels,  $pp \rightarrow Z' \rightarrow \ell^+\ell^-$  ( $\ell = e, \mu$ ), one would be able to measure immediately the mass  $M_{Z'}$ , the width  $\Gamma_{tot}$  and the total cross section  $\sigma_{\ell\ell}$ . However,  $\sigma_{\ell\ell} = \sigma(pp \rightarrow Z')B$  is *not* a useful diagnostic probe for the  $Z'$  gauge couplings to quarks and leptons. While  $\sigma(pp \rightarrow Z')$ , the total production cross section, can be calculated to within a few percent for given  $Z'$  couplings, the branching ratio into leptons,  $B \equiv \Gamma(Z' \rightarrow \ell^+\ell^-)/\Gamma_{tot}$ , is model dependent; it depends on the contribution of exotic fermions and supersymmetric partners to the  $Z'$  width, and thus it cannot be useful as a diagnostic test for the  $Z'$  gauge couplings. However, it would be a useful indirect probe for the existence of the exotic fermions or superpartners. On the other hand, from measurements of the total width  $\Gamma_{tot}$ , and  $\sigma_{\ell\ell}$  one obtains  $\sigma\Gamma(Z' \rightarrow \ell^+\ell^-) \equiv \sigma B\Gamma_{tot}$ , which probes the absolute magnitude of the gauge couplings.

In the following we will address signals which probe *relative strengths* of  $Z'$  gauge couplings. The forward-backward asymmetry [20] in the main production channel  $pp \rightarrow Z' \rightarrow \ell^+\ell^-$  ( $\ell = e$  or  $\mu$ ).<sup>4</sup> was the first recognized probe for the gauge couplings at future hadron colliders. Since then a number of new, complementary probes were proposed [36, 42]–[50].

The nature of such probes can be classified according to the type of channel in which they can be measured:

**(Ia)** *The main production channels:*

- (A)** Forward-backward asymmetry [20],
- (B)** Ratio of cross-sections in different rapidity bins [34],
- (C)** Corresponding asymmetries if proton polarization were available [44].

**(Ib)** *Other two-fermion final state channels:*

- (D)** Measurements of the  $\tau$  polarization in the  $pp \rightarrow Z' \rightarrow \tau^+\tau^-$  channel [43],
- (E)** Measurements of the cross section in the  $pp \rightarrow Z' \rightarrow jet\ jet$  channel [50, 51].

**(II)** *The four-fermion final state channels:*

- (F)** Rare decays  $Z' \rightarrow W\ell\nu_\ell$  [52, 42],
- (G)** Associated productions  $pp \rightarrow Z'V$  with  $V = (Z, W)$  [47] and  $V = \gamma$  [48].

Probes under (Ia) constitute distributions, *i.e.*, “refinements”, in the main production channels. The forward-backward asymmetry (A) is the cleanest one, probing a particular combination of quark and lepton couplings. On the other hand, the rapidity ratio (B) [34] was recognized as a useful complementary probe separating the  $Z'$  couplings to the  $u$  and  $d$  quarks due to the harder valence  $u$ -quark distribution in the proton relative to the  $d$ -quark. Probes (C) are useful ones if proton polarization were available at future hadron colliders. In addition, better knowledge of the polarized spin distribution functions for quarks is needed.

For probes in other than the main production channels (Ib) the background can be large. For (E) recent studies indicate [49, 50, 51] that the large QCD background may be overcome with appropriate kinematic cuts, excellent dijet mass resolution, and detailed knowledge of the QCD backgrounds. (D) provides another interesting

---

<sup>4</sup>See also Ref. [41].



possibility to address the  $Z'$  lepton couplings, while (E) is the only probe available for the left-handed quark coupling [47].

Probes in the four-fermion final state channels (II) have suppressed rates compared to the two-fermion channels (Ia) and (Ib). In these cases one hopes to have enough statistics, and no attempt to study distributions seems to be possible.

Rare decays  $Z' \rightarrow f_1 \bar{f}_2 V$ , with ordinary gauge bosons  $V = (Z, W)$  emitted by Bremsstrahlung from one of the fermionic ( $f_{1,2}$ ) legs turn out to have sizable statistics [42], which is due to a double logarithmic enhancement [42], closely related to collinear and infrared singularities of gauge theories. They were studied in detail in Refs. [42, 45, 46]. A background study [42, 47] of such decays revealed that the only useful mode<sup>5</sup> without large standard model and QCD backgrounds is (F):  $Z' \rightarrow W \ell \nu_\ell$  and  $W \rightarrow \text{hadrons}$ , with the imposed cut  $m_{T\ell\nu_\ell} > 90$  GeV on the transverse mass of the  $\ell\nu_\ell$ . (This assumes that there is a sufficiently high efficiency for the reconstruction of  $W \rightarrow \text{hadrons}$  in events tagged by an energetic lepton. Further study of the QCD background and the jet reconstruction for such processes is needed.) The same mode with  $W \rightarrow \ell\nu_\ell$  may also be detectable [45] if appropriate cuts are applied.<sup>6</sup> These modes probe a left-handed leptonic coupling.

Associated productions (F) turn out to be relatively clean signals [47] with slightly smaller statistics than rare decays. They probe a particular combination of the gauge couplings to quarks and are thus complementary to rare decays.

At the LHC the above signals are feasible diagnostic probes for  $M_{Z'} \lesssim 1-2$  TeV. For diagnostic study of  $Z'$  couplings large luminosity is important. For higher  $Z'$  masses the number of events drops rapidly. For  $M_{Z'} \simeq 2$  TeV, the statistical errors on forward-backward asymmetry (A), the rapidity ratio (B), and rare decays (F) increase by a factor of 4, while those on associated productions (G) increase by a factor of 3. A reasonable discrimination between models and determination of the couplings may still be possible, primarily from the forward-backward asymmetry and the rapidity ratio. However, for  $M_{Z'} \simeq 3$  TeV the statistical errors on the first three quantities are larger by a factor of 13 than for 1 TeV, and there are not enough events expected for the associated production to allow a meaningful measurement. For  $M_{Z'} \leq 3$  TeV, there is therefore little ability to discriminate between models.

### 5.1.1 Determination of Gauge Couplings at the LHC

We next examine how well the various  $Z'$  couplings could be extracted from the above probes. We will mainly concentrate on probes (A), (B), (F) and (G), which seem to be the most feasible. For definiteness, we consider the statistical uncer-

<sup>5</sup> $Z' \rightarrow Z \ell^+ \ell^-$  does not significantly discriminate between models.

<sup>6</sup> A possibility of gaining useful information from  $Z' \rightarrow Z \nu_\ell \bar{\nu}_\ell$  [42, 47, 46] was also addressed in Ref. [53].

tainties for  $M_{Z'} = 1$  TeV at the LHC. Eventually, the uncertainties associated with the detector acceptances and systematic errors will have to be taken into account.

In the following we assume family universality, neglect  $Z - Z'$  mixing and assume  $[Q', T_i] = 0$ , which holds for  $SU_2 \times U_1 \times U_1'$  and LR models. Here,  $Q'$  is the  $Z'$  charge and  $T_i$  are the  $SU_{2L}$  generators.<sup>7</sup>

The relevant quantities [47, 34] to distinguish different theories are the charges,  $\hat{g}_{L2}^u = \hat{g}_{L2}^d \equiv \hat{g}_{L2}^q$ ,  $\hat{g}_{R2}^u$ ,  $\hat{g}_{R2}^d$ ,  $\hat{g}_{L2}^\nu = \hat{g}_{L2}^e \equiv \hat{g}_{L2}^\ell$ , and  $\hat{g}_{R2}^\ell$ , and the gauge coupling strength  $g_2$ . The signs of the charges will be hard to determine at hadron colliders. Thus the following four “normalized” observables can be probed [47]:

$$\gamma_L^\ell \equiv \frac{(\hat{g}_{L2}^\ell)^2}{(\hat{g}_{L2}^\ell)^2 + (\hat{g}_{R2}^\ell)^2}, \quad \gamma_L^q \equiv \frac{(\hat{g}_{L2}^q)^2}{(\hat{g}_{L2}^q)^2 + (\hat{g}_{R2}^q)^2}, \quad \tilde{U} \equiv \frac{(\hat{g}_{R2}^u)^2}{(\hat{g}_{L2}^q)^2}, \quad \tilde{D} \equiv \frac{(\hat{g}_{R2}^d)^2}{(\hat{g}_{L2}^q)^2}. \quad (18)$$

The values of  $\gamma_L^\ell$ ,  $\gamma_L^q$ ,  $\tilde{U}$ , and  $\tilde{D}$  for the above models are listed in Table 3.

Table 3: Values of the “normalized” couplings (1) for the typical models and the statistical error-bars as determined from probes at the LHC ( $\sqrt{s} = 14$  TeV,  $\mathcal{L}_{int} = 100$  fb<sup>-1</sup>).  $M_{Z'} = 1$  TeV.

	$\chi$	$\psi$	$\eta$	LR
$\gamma_L^\ell$	$0.9 \pm 0.016$	$0.5 \pm 0.02$	$0.2 \pm 0.012$	$0.36 \pm 0.007$
$\gamma_L^q$	0.1	0.5	0.8	0.04
$\tilde{U}$	$1 \pm 0.16$	$1 \pm 0.14$	$1 \pm 0.08$	$37 \pm 6.6$
$\tilde{D}$	$9 \pm 0.57$	$1 \pm 0.22$	$0.25 \pm 0.16$	$65 \pm 11$

The forward-backward asymmetry (A) is defined as:

$$A_{FB} = \frac{\left[ \int_0^{y_{max}} - \int_{-y_{max}}^0 \right] [F(y) - B(y)] dy}{\int_{-y_{max}}^{y_{max}} [F(y) + B(y)] dy}, \quad (19)$$

while the rapidity ratio (B) is defined as [34]:

$$r_{y_1} = \frac{\int_{-y_1}^{y_1} [F(y) + B(y)] dy}{\left( \int_{-y_{max}}^{-y_1} + \int_{y_1}^{y_{max}} \right) [F(y) + B(y)] dy}. \quad (20)$$

Here  $F(y) \pm B(y) = \left[ \int_0^1 \pm \int_{-1}^0 \right] d \cos \theta (d^2 \sigma / dy d \cos \theta)$ , where  $y$  is the  $Z'$  rapidity and  $\theta$  is the  $\ell^-$  angle in the  $Z'$  rest frame. The rapidity range is from  $\{-y_{max}, y_{max}\}$ .  $y_1$  is chosen in a range  $0 < y_1 < y_{max}$  so that the number of events in the two bins

<sup>7</sup> For conventions in the neutral current interactions see Ref. [54].

are comparable. At the LHC ( $y_{max} \simeq 2.8$ ) for  $M_{Z'} \simeq 1$  TeV, and  $y_1 = 1$  turns out to be an appropriate choice. For rare decays (F) one defines [42]:

$$r_{\ell\nu W} \equiv \frac{B(Z' \rightarrow W \ell \nu_\ell)}{B(Z' \rightarrow \ell^+ \ell^-)} , \quad (21)$$

in which one sums over  $\ell = e, \mu$  and over  $W^+, W^-$ . For the associated productions (G) one defines [47] the ratios:

$$R_{Z'V} = \frac{\sigma(pp \rightarrow Z'V)B(Z' \rightarrow \ell^+ \ell^-)}{\sigma(pp \rightarrow Z')B(Z' \rightarrow \ell^+ \ell^-)} , \quad (22)$$

with  $V = (Z, W)$  decaying into leptons and quarks, and  $V = \gamma$  with an imposed  $p_{T\gamma} \geq 50$  GeV cut.  $\ell$  includes both  $e$  and  $\mu$ .

Statistical errors and explicit dependence of the above probes on the couplings (18) for  $M_{Z'} = 1$  TeV are given in Table 4. The EHLQ distribution functions [25], set 1, are used. One also assumes that the  $Z'$  only decays into the ordinary three families of quarks and leptons. Realistic fits, which include updated structure functions, kinematic cuts, and detector acceptances are expected to give larger uncertainties for the couplings.<sup>8</sup>

The error bars turn out to be sufficiently small to distinguish between models. The six quantities  $A_{FB}$ ,  $r_{y_{1,2}}$ ,  $r_{\ell\nu W}$ , and  $R_{Z'V}$  with ( $V = Z, W, \gamma$ ) yield significant information on three ( $\gamma_L^\ell$ ,  $\tilde{U}$  and  $\tilde{D}$ ) out of four normalized gauge couplings of ordinary fermions to the  $Z'$ . The fourth normalized coupling  $\gamma_L^q$  could be determined [47] by a measurement of the branching ratio  $B(Z' \rightarrow q\bar{q})$ . It turns out [50], however, that for  $M_{Z'} \geq 1$  TeV and the typical models (except the SSM), the  $Z'$  gauge couplings are too small to allow for determination of  $\gamma_L^q$  with sufficient precision at the LHC.

To study the precision to which these couplings could be determined, a combined  $\chi^2$  analysis of these observables has been performed, updating the earlier analysis of Ref. [34]. Only the statistical uncertainties have been included and correlations between the observables have been ignored. The results are given in Table 3. In particular,  $\gamma_L^\ell$  can be determined very well (between 2% and 8% for the  $\chi$ ,  $\psi$ , and  $\eta$  models), primarily due to the small statistical error for the rare decay mode  $Z' \rightarrow W \ell \nu_\ell$ . On the other hand the quark couplings have larger uncertainties, typically 20%. In Fig. 4, 90% confidence level ( $\Delta\chi^2 = 6.3$ ) contours<sup>9</sup> are given in a three-dimensional plot for  $\tilde{U}$  versus  $\tilde{D}$  versus  $\gamma_L^\ell$  for the  $\eta$ ,  $\psi$  and  $\chi$  models. The  $LR$  model has  $\tilde{U}$  and  $\tilde{D}$  in a different region of the parameter space (see Table 3). From Fig. 4 it is clear that one can distinguish well between different models.

<sup>8</sup>Table 3 updates the results of Ref. [34] where the uncertainties are given for  $\sqrt{s} = 16$  TeV. In addition, in Table 4 more optimistic assumptions on the branching ratios are used.

<sup>9</sup> The 90% confidence level contours for projections on the more familiar two-dimensional parameter subspaces correspond to  $\Delta\chi^2 = 4.6$ .

Table 4: a) displays the dependence of the probes on the couplings [defined in (5.1)] at the LHC ( $\sqrt{s} = 14$  TeV,  $\mathcal{L}_{int} = 100 \text{ fb}^{-1}$ ) for  $M_{Z'} = 1$  TeV. The numerical values (with statistical errors) of the corresponding probes for typical models are given in b).

a)

$A_{FB}$	$\frac{.387(2\gamma_L^l - 1) \times (1 - .753\tilde{U} - .247\tilde{D})}{1 + .684\tilde{U} + .316\tilde{D}}$
$r_{y_1}$	$1.796 \frac{1 + .652\tilde{U} + .348\tilde{D}}{1 + .736\tilde{U} + .264\tilde{D}}$
$A_{FB_{y_1}}$	$.726 \frac{1 - .731\tilde{U} - .269\tilde{D}}{1 - .769\tilde{U} - .231\tilde{D}}$
$B_{qq}$	$\gamma_L^l (2 + \tilde{U} + \tilde{D})$
$r_{l\nu W}$	$0.067 \gamma_L^l$
$R_{Z'Z}$	$\frac{10^{-3}(7.55 + .924\tilde{U} + 0.098\tilde{d})}{1 + .684\tilde{U} + .316\tilde{D}}$
$R_{Z'W}$	$\frac{24.53 \times 10^{-3}}{1 + .684\tilde{U} + .316\tilde{D}}$
$R_{Z'\gamma}$	$\frac{5.38 \times 10^{-3}(1 + .896\tilde{U} + .104\tilde{D})}{1 + .684\tilde{U} + .316\tilde{D}}$

b)

	$\chi$	$\psi$	$\eta$	$LR$
$A_{FB}$	$-.1346 \pm .0063$	$0 \pm 0.0087$	$-.0244 \pm .0080$	$.1025 \pm .0059$
$r_{y_1}$	$2.091 \pm .020$	$1.796 \pm .023$	$1.732 \pm .020$	$1.891 \pm .017$
$A_{FB_{y_1}}$	$.85 \pm .08$		$.85 \pm .58$	$.74 \pm .09$
$r_{l\nu W}$	$.059 \pm .0013$	$.033 \pm .0014$	$.013 \pm .0008$	$.023 \pm .0008$
$R_{Z'Z}$	$2.08 \pm .21$	$4.24 \pm .4$	$4.88 \pm .4$	$1.03 \pm .13$
$R_{Z'W}$	$5.41 \pm .33$	$12.07 \pm .68$	$13.99 \pm .67$	$.538 \pm .097$
$R_{Z'\gamma}$	$3.28 \pm .26$	$5.23 \pm .45$	$6.02 \pm .44$	$4.9 \pm .29$

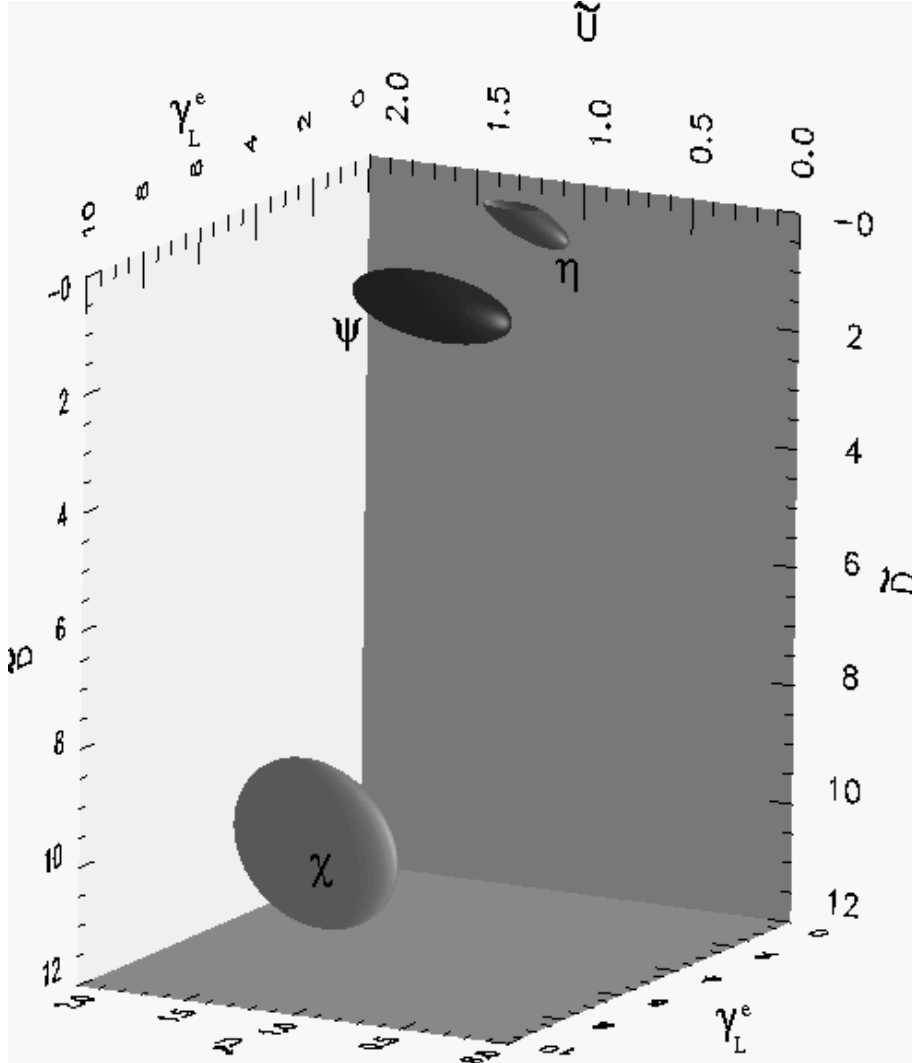


Figure 4: 90% confidence level ( $\Delta\chi^2 = 6.3$ ) contours for the  $\chi$ ,  $\psi$  and  $\eta$  models are plotted for  $\tilde{U}$ , versus  $\tilde{D}$ , versus  $\gamma_L^e$ . The input data are for  $M_{Z'} = 1$  TeV at the LHC ( $\sqrt{s} = 14$  TeV and  $\mathcal{L}_{int} = 100 \text{ fb}^{-1}$ ) and include statistical errors only.

The LHC can also address  $W'$  diagnostics for  $M_{W'} \lesssim 1 - 2$  TeV. In particular, indirect information on the Higgs sector is possible from  $W' \rightarrow WZ$  decays. The ratio  $M_{W'}/M_{Z'}$  (an analog of the  $\rho$  parameter in the standard model) would also yield information on the nature of the Higgs sector.  $W'$  decays into right-handed neutrinos (and other exotics) would yield additional useful information on the  $W'$ .

$W'$  gauge couplings to ordinary quarks and leptons is possible by studying the forward-backward asymmetry and the rapidity ratios in the main production channel  $pp \rightarrow W' \rightarrow \ell\nu_\ell$  ( $\ell = e, \mu$ ) as well as associated productions (*e.g.*,  $pp \rightarrow W'Z$ ) and rare decays (*e.g.*,  $W' \rightarrow Z\ell^+\ell^-$ ) in the corresponding four-fermion final state channels.<sup>10</sup> While the forward-backward asymmetry in the main production channels  $pp \rightarrow W' \rightarrow \ell\nu_\ell$  ( $\ell = e, \mu$ ) probes some combination of gauge couplings, it does not distinguish  $\hat{g}_{L2}$  from  $\hat{g}_{R2}$  couplings. On the other hand, rare decays  $W'^{\pm} \rightarrow W\ell^+\ell^-$  and associated productions  $pp \rightarrow W'^{\pm}W^{\mp}$  are strongly suppressed [42, 36, 47] if  $W'$  has only  $\hat{g}_{R2}$  couplings, as in the LR symmetric models. In models where  $W'$  has  $\hat{g}_{L2}$  couplings, *e.g.*, the so-called ununified standard model (UNSM) [12], the corresponding rates are, however, not suppressed; primarily due to the larger gauge couplings of the  $W'$ , the corresponding rates allow for determination of  $\hat{g}_{L2}$  couplings for  $M_{W'}$  up to around 3 TeV. Note, however, that for these processes it is difficult to disentangle the contributions from the direct coupling of the  $W'$  to ordinary fermions and the non-Abelian coupling of the  $W'$  to ordinary gauge bosons.

For  $M_{Z'} \simeq 2$  TeV a reasonable discrimination between models and determination of the couplings may still be possible, primarily from the forward-backward asymmetry and the rapidity ratio. However, for  $M_{Z'} \simeq 3$  TeV there is little ability to discriminate between models.

## 5.2 New Gauge Boson Diagnostics at the NLC

If a  $Z'$  were produced on shell at the NLC it would be relatively straightforward to determine its properties. On the other hand, if it is far off-shell (a more likely possibility) its properties could be deduced [56, 57] through interference effects of the  $Z'$  propagator with the  $\gamma$  and  $Z$  propagator. In this case the various observables described in the previous section to deduce the existence of a  $Z'$  can also be used to extract [58, 59] its couplings to quarks and leptons, yielding information complementary to the LHC. Such couplings can in turn allow one to determine the nature of the underlying extended gauge structure [56, 60].

Since the photon couplings are only vector-like and the  $\ell$  couplings to  $Z$  have the property  $\hat{g}_{L1}^\ell \simeq -\hat{g}_{R1}^\ell$  it turns out that the probes in the two-fermion final state channels single out the  $Z'$  leptonic couplings primarily in the combinations  $\hat{g}_{L2}^\ell \pm \hat{g}_{R2}^\ell$ . To trace the combinations of the normalized charges to which the probes are sensitive, it is advantageous to choose either of the two combinations to

---

<sup>10</sup>See for example Ref. [55].

normalize the charges. We choose the  $\hat{g}_{L2}^\ell - \hat{g}_{R2}^\ell$  combination, which turns out to be a convenient choice for the typical models used in the analysis. We then define the following four independent “normalized” charges:

$$P_V^\ell = \frac{\hat{g}_{L2}^\ell + \hat{g}_{R2}^\ell}{\hat{g}_{L2}^\ell - \hat{g}_{R2}^\ell}, \quad P_L^q = \frac{\hat{g}_{L2}^q}{\hat{g}_{L2}^\ell - \hat{g}_{R2}^\ell}, \quad P_R^{u,d} = \frac{\hat{g}_{R2}^{u,d}}{\hat{g}_{L2}^q}. \quad (23)$$

Their values are given for the typical models in Table 5. In addition, the probes in the two-fermion final state channels are sensitive to the following ratio of an overall gauge coupling strength divided by the “reduced”  $Z'$  propagator:

$$\epsilon_A = (\hat{g}_{L2}^\ell - \hat{g}_{R2}^\ell)^2 \frac{g_2^2}{4\pi\alpha} \frac{s}{M_{Z'}^2 - s}. \quad (24)$$

Here  $\alpha$  is the fine structure constant. Note again that the four normalized charges (23) and  $\epsilon_A$  (24) can be replaced with an equivalent set by choosing  $\hat{g}_{L2}^\ell + \hat{g}_{R2}^\ell$  to normalize the couplings.

Table 5: Values of the couplings (23) and (24) for the typical models and statistical error-bars as determined from probes at the NLC ( $\sqrt{s} = 500$  GeV,  $\mathcal{L}_{int} = 20$  fb $^{-1}$ ).  $M_{Z'} = 1$  TeV. 100% heavy flavor tagging efficiency and 100% longitudinal polarization of the electron beam is assumed for the first set of error bars, while the error bars in parentheses are for the probes without polarization.

	$\chi$	$\psi$	$\eta$	$LR$
$P_V^\ell$	$2.0 \pm 0.08$ (0.26)	$0.0 \pm 0.04$ (1.5)	$-3.0 \pm 0.5$ (1.1)	$-0.15 \pm 0.018$ (0.072)
$P_L^q$	$-0.5 \pm 0.04$ (0.10)	$0.5 \pm 0.10$ (0.2)	$2.0 \pm 0.3$ (1.1)	$-0.14 \pm 0.037$ (0.07)
$P_R^u$	$-1.0 \pm 0.15$ (0.19)	$-1.0 \pm 0.11$ (1.2)	$-1.0 \pm 0.15$ (0.24)	$-6.0 \pm 1.4$ (3.3)
$P_R^d$	$3.0 \pm 0.24$ (0.51)	$-1.0 \pm 0.21$ (2.8)	$0.5 \pm 0.09$ (0.48)	$8.0 \pm 1.9$ (4.1)
$\epsilon_A$	$0.071 \pm 0.005$ (0.018)	$0.121 \pm 0.017$ (0.02)	$0.012 \pm 0.003$ (0.009)	$0.255 \pm 0.016$ (0.018)

One should contrast the above choice of the normalized couplings with those chosen for the LHC. Recall that couplings (18) probed by the LHC, do not determine couplings (23) and (24) unambiguously. In particular, determination of  $\gamma_L^\ell$ ,  $\tilde{U}$  and  $\tilde{D}$  at the LHC would yield an eight-fold ambiguity for the corresponding three couplings in (23) and (24).

The probes at the NLC constitute the cross sections and corresponding asymmetries in the two-fermion final state channels,  $e^+e^- \rightarrow f\bar{f}$ . Due to the interference of the  $Z'$  propagator with the photon and the  $Z$  propagators such probes are sensitive to the four normalized charges in (23) as well as to the parameter  $\epsilon_A$  (24). The tree-level expressions for such probes can be written explicitly in terms of seven generalized charges, which are given in Ref. [56].

The analysis is based on the following probes:

$$\sigma^\ell, \quad R^{had} = \frac{\sigma^{had}}{\sigma^\ell}, \quad A_{FB}^\ell. \quad (25)$$

In the case that longitudinal polarization of the electron beam is available there are additional probes:

$$A_{LR}^{\ell,had}, \quad A_{LR,FB}^\ell. \quad (26)$$

Here  $\sigma$ ,  $A_{FB}$ ,  $A_{LR}$  and  $A_{LR,FB}$  refer to the corresponding cross sections, forward-backward asymmetries, left-right (polarization) asymmetries and left-right-forward-backward asymmetries, respectively. The superscripts  $\ell$  and  $had$  refer to all three leptonic channels (considering only  $s$ -channel exchange for electrons) and to all hadronic final states, respectively. The above quantities help to distinguish among different models [56]; however, they do not yield information on all the  $Z'$  couplings. In particular  $\sigma^\ell$  and  $A_{FB}^\ell$  probe  $\epsilon_A$  and the magnitude of  $P_V^\ell$ , but not its sign. On the other hand,  $R^{had}$  provides additional information on one linear combination of the normalized quark couplings. If polarization is available,  $A_{LR}^\ell$  and  $A_{LR,FB}^\ell$  are excellent probes for  $P_V^\ell$  (including its sign), while  $A_{LR}^{had}$  yields information on another linear combination of the quark couplings.

LEP analyses [61] show that current  $e^+e^-$  colliders allow for an efficient tagging of charm ( $c$ ) and bottom ( $b$ ) final states. The large momentum and the nature of the ( $c, b$ ) lifetimes allow for flavor tagging by ‘flight’ identification. At *LEP* there are three different methods for  $b$  identification, based on lepton tagging, event shape and lifetime tagging. On the other hand *NLC* detectors would be (at least) as good as the corresponding *LEP* ones. In addition, a larger energy of jets at the *NLC* would imply a cleaner signature. We therefore assume that at the *NLC* an efficient tagging of the heavy flavors ( $c, b, t$ ) would be available. This in turn provides an additional set of observables:

$$R^f = \frac{\sigma^f}{\sigma^\ell}, \quad A_{FB}^f; \quad f = c, b, t, \quad (27)$$

and with polarization available:

$$A_{LR}^f, \quad A_{LR,FB}^f; \quad f = c, b, t, \quad (28)$$

where the superscript refers to the corresponding heavy flavors.

### 5.2.1 Determination of Gauge Couplings at the NLC

We now study how well one can determine the couplings defined in Section 5.2 at the *NLC*. The effects of a heavy  $Z'$  far off-shell are expected to be small and comparable to the electro-weak radiative corrections [56]. The latter ones are dominated by initial state radiation, which can be greatly reduced by applying a cut on the maximum photon energy to exclude  $Z$  production. With such a cut



the tree-level expressions are a reasonably good approximation to the different observables. Since our present goal is to explore the sensitivity of the  $Z'$  couplings, it is sufficient to neglect the remaining radiative corrections. Of course, if a new  $Z'$  is actually discovered a realistic fit should include full radiative corrections as well as experimental cuts and detector acceptances.

Only statistical errors for the observables are included and error correlations for the input parameters are neglected in the analysis. In addition, experimental cuts and detector acceptances are not included either. The results should thus be interpreted as a limit on how precisely the couplings can be determined for each model for the given c.m. energy and the integrated luminosity of the NLC. Realistic fits are expected to give larger uncertainties for the couplings.

For  $M_{Z'} = 1$  TeV the couplings for the typical models and the corresponding statistical uncertainties are given in Table 5. In Fig. 5, 90% confidence level ( $\Delta\chi^2 = 6.3$ ) regions are given in a three-dimensional plot of  $P_R^u$  versus  $P_R^d$  versus  $P_V^\ell$  for the  $\chi$ ,  $\psi$  and  $\eta$  models (the  $LR$  model is in a different region of parameter space). 100% efficiency for heavy flavor tagging (probes) and 100% longitudinal polarization of the initial electron beam has been assumed. Relative error bars are about a factor of 2 larger than the corresponding ones at the LHC. The  $Z'$  charges can be determined to around 10 – 20%.

In the case of smaller, say, 25%, heavy flavor tagging efficiency and in the case that the electron beam polarization is reduced to, say, 50%, the determination of the couplings is poorer, though still useful (see Ref. [58].).

The diagnostic power of the  $NLC$  for the  $Z'$  couplings decreases drastically for  $M_{Z'} \gtrsim 1$  TeV. *E.g.*, for  $M_{Z'} = 2$  TeV, the uncertainties for the couplings in the typical models are 100%, and thus a model-independent determination of such couplings is difficult at the NLC. For  $M_{Z'} \sim 2$  TeV, the uncertainties for the couplings in the typical models are too large to discriminate between models.

Given the  $W'$  limits achievable at the upgraded Tevatron, it is unlikely that  $W'$  diagnostics will be possible at the 500 GeV NLC.

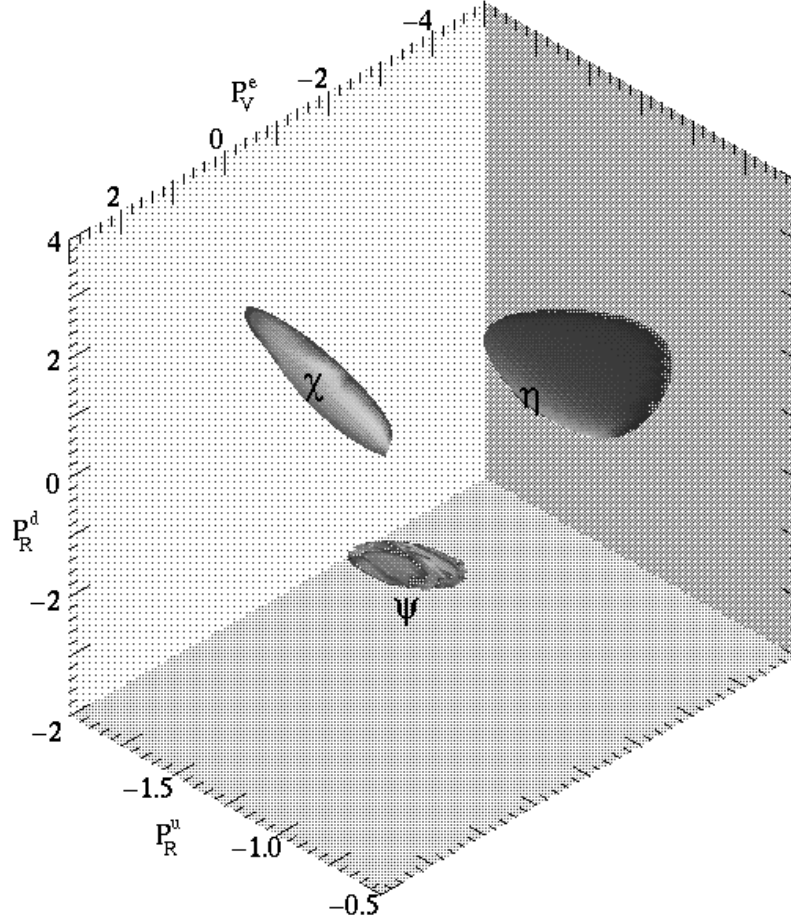


Figure 5: 90% confidence level ( $\Delta\chi^2 = 6.3$ ) regions for the  $\chi, \psi$  and  $\eta$  models with  $M_{Z'} = 1$  TeV are plotted on  $P_R^u$  versus  $P_R^d$  versus  $P_V^l$  at the *NLC*.

### 5.3 Comparison of the Diagnostic Power of the NLC and the LHC

The couplings (18) that are probed directly at the LHC are not sensitive to the relative signs of the  $Z'$  charges. This in turn implies that couplings (23), which are observed directly at the *NLC*, are probed with a few-fold ambiguity at the *LHC*. In Table 6 we collect the errors expected at the *LHC* for the three couplings  $P_V^\ell$ ,  $P_R^u$  and  $P_R^d$ . We again choose the typical models and  $M_{Z'} = 1$  TeV. There is an eight-fold ambiguity in determination of these couplings; only the first value of  $P_V^\ell$ ,  $P_R^u$  and  $P_R^d$  corresponds to the actual values of the typical models. Note, however, that the error-bars are typically a factor of  $\sim 2$  smaller than those at the NLC (compare Tables 5 and 6).

Table 6: Values of three (out of four) couplings which are probed (indirectly) at the LHC. The error-bars indicate how well these couplings can be measured at the LHC ( $\sqrt{s} = 14$  TeV and  $\mathcal{L}_{int} = 100 \text{ fb}^{-1}$ ) for the typical models with  $M_{Z'} = 1$  TeV. There is a two-fold ambiguity for each of the couplings. Only the first number corresponds to the actual value of the coupling of the particular model.

	$\chi$	$\psi$	$\eta$	$LR$
$P_V^\ell$	$2 \pm 0.13$	$0 \pm 0.03$	$-3 \pm 0.15$	$-0.148 \pm 0.007$
	$0.5 \pm 0.03$	$\infty \pm \infty$	$-0.333 \pm 0.017$	$-7 \pm 0.36$
$P_R^u$	$\mp 1 \pm 0.08$	$\mp 1 \pm 0.07$	$\mp 1 \pm 0.04$	$\mp 6.04 \pm 0.27$
$P_R^d$	$\pm 3 \pm 0.09$	$\mp 1 \pm 0.11$	$\pm 0.5 \pm 0.16$	$\pm 8.04 \pm 0.68$

In Fig. 6 we plot 90% confidence level ( $\Delta\chi^2 = 6.3$ ) regions for the  $\chi$ ,  $\psi$  and  $\eta$  models as  $P_R^u$  versus  $P_R^d$  versus  $P_V^\ell$  at the *LHC*. While the error-bars are small, the figure displays a few-fold ambiguity for the value of the couplings (23) (additional ambiguities are off the scale of the plot). At the NLC the error-bars are on the average larger, but the ambiguity in the value of the couplings is now removed. Thus, the LHC and the NLC are complementary and together have the potential to uniquely determine the couplings with small error-bars.

Finally, we would also like to point out that the determination of  $Z'$  couplings to quarks and leptons would in turn allow the determination of the nature of the underlying extended gauge structure [60]. As a prime example one can choose the  $E_6$  group. In this case two discrete constraints on experimentally determined couplings have to be satisfied. If so, the couplings would then uniquely determine the two parameters,  $\theta_{E_6}$  and  $\kappa$ , which fully specify the nature of the  $Z'$  within  $E_6$ . If the  $Z'$  is part of the  $E_6$  gauge structure, then for  $M_{Z'} = 1$  TeV  $\theta_{E_6}$  and

$\kappa$  could be determined to around 10% at the future colliders. In particular, one would be able to separate the  $LR$  symmetry breaking chains from the  $SM \times U(1)'$  chains. The NLC provides a unique determination of the two constraints as well as of  $\theta_{E_6}$  and  $\kappa$ , though with slightly larger error bars than at the LHC. On the other hand, since the LHC primarily determines three out of four normalized couplings, it provides weaker constraints for the underlying gauge structure. For more details see Ref. [60].

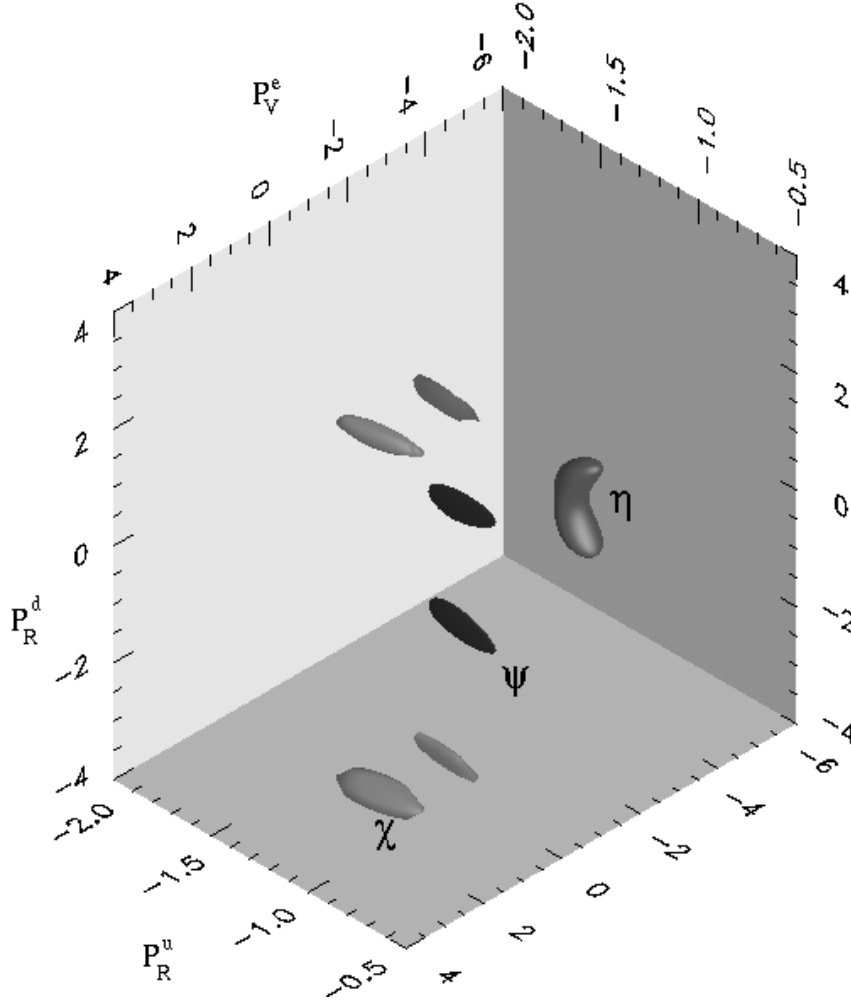


Figure 6: 90% confidence level ( $\Delta\chi^2 = 6.3$ ) regions for the  $\chi$ ,  $\psi$ , and  $\eta$  models with  $M_{Z'} = 1$  TeV are plotted for  $P_R^u$  versus  $P_R^d$  versus  $P_V^l$  at the *LHC*. The figure reflects a few-fold ambiguity in the determination of these couplings at the *LHC*.

## 6 Conclusions and Recommendations

Among the facilities operating in the up-coming decade TEVATRON offers the highest discovery reach for new heavy gauge bosons with masses up to 700–900 GeV range.

In the longer term, future hadron colliders, *i.e.*, different upgraded versions of the TEVATRON and the LHC, as well as a high luminosity  $e^+e^-$  collider, *i.e.*, the NLC, would significantly improve limits on the heavy gauge boson masses. For the typical models such limits are in the 1–2 TeV region for the TEVATRON upgrades, in the 4–5 TeV region for the LHC, and roughly  $2-10 \times \sqrt{s}$  for the NLC with  $50 \text{ fb}^{-1}$ .

The LHC and a high luminosity 500 GeV  $e^+e^-$  collider have discovery limits for  $Z'$  which are in many cases comparable. Both facilities have strengths and weakness. The limits obtained from the LHC are robust, in the sense that they are obtained from a direct measurement with little background, but the sensitivity is dependent on the total width of the  $Z'$ , which depends on assumptions of the particle content of the model. Limits obtained for the NLC are indirect, based on statistical deviations from the Standard Model, and are therefore more sensitive to having the systematic errors under control. However, they do not depend on the unknown particle content of the model. With these caveats we would still consider, for the purposes of discovering extra gauge bosons, the LHC to be the machine of choice.

We have also explored the diagnostic power of the LHC and the NLC for a model independent determination of  $Z'$  couplings to quarks and leptons, once a  $Z'$  is discovered. In addition, the determination of such  $Z'$  couplings would in turn allow one to determine the nature of the underlying extended gauge structure. At the NLC, efficient heavy flavor tagging and longitudinal polarization of the electron beam provide probes in the two-fermion final state channels, which are sensitive to the magnitude as well as the relative signs of *all* the  $Z'$  charges to quarks and leptons. For  $M_{Z'} \lesssim 1 \text{ TeV}$ , such couplings would be determined to about 10–20 % for a class of typical models. If polarization were not available, the determination of the  $Z'$  couplings would be marginal, since the error-bars increase by a factor of 2–10. Without heavy flavor tagging very little can be learned about the quark couplings.

The LHC is complementary in nature; while it primarily allows for the determination of the magnitude of only three out of four normalized couplings, the corresponding errors are typically a factor of  $\sim 2$  smaller than those for the NLC for typical models with  $M_{Z'} = 1 \text{ TeV}$ . In addition, the LHC would measure  $M_{Z'}$  directly and would allow for a determination of an overall strength of the  $Z'$  gauge coupling to fermions. This is in contrast to the NLC which, for the fixed c.m. energy, primarily determines only the ratio of an overall  $Z'$  gauge coupling strength and  $M_{Z'}$ .

The two machines possess complementary diagnostic power for the model independent determination of the  $Z'$  couplings to quarks and leptons. In conjunction, they allow for determination of the  $M_{Z'}$ , an overall  $Z'$  gauge coupling strength as well as a unique determination of *all* the quark and lepton charges with error bars in the 10–20% range, provided  $M_{Z'} \lesssim 1\text{--}2$  TeV. In addition, at the LHC  $W'$  diagnostics is possible for  $M_{W'} \leq 1\text{--}2$  TeV.

A final observation is that if the DI-TEVATRON were running prior to turning on of the LHC, the non discovery of an extra gauge boson at the DI-TEVATRON would imply that the  $Z'$  is too heavy to allow for diagnostic study of its properties at the LHC and/or the NLC.

## Acknowledgment

We would like to thank P. Langacker for help with updating the results for the global fits and other results as well as for the careful reading of the manuscript. M.C. thanks F. del Aguila for useful discussions and S.G. thanks T. Rizzo for helpful communications.

## References

- [1] R.W. Robinett, Phys. Rev. **D26** 2388 (1982); R.W. Robinett and J.L. Rosner, *ibid* **25** 3036 (1982); *ibid* **D26** 2396 (1982) P. Langacker, R. W. Robinett, and J.L. Rosner, Phys. Rev. **D30**, 1470 (1984).
- [2] M. Green and J. Schwarz, Phys. Lett. **149B**, 117(1984); Phys. Lett. **151B**,21(1985); D. Gross *et al.*, Phys. Rev. Lett. **54**, 502 (1985); E. Witten, Phys. Lett. **155B** 1551 (1985); Nucl. Phys. **B258** 75 (1985); P. Candelas *et al.*, *ibid* **B258** 46 (1985); M. Dine *et al.*, Nucl. Phys. **B259**, 549 (1985); J. Ellis *et al.*, CERN Report CERN-TH-4350/86 (1986; unpublished); J.D. Breit, B.A. Ovrut, and G.C. Segrè, Phys. Lett. **158B**, 33 (1985); P. Candelas *et al.*, Nucl. Phys. **B258**, 46 (1985); S. Cecotti *et al.*, *ibid* **156B**, 318 (1985).
- [3] For a review and original references see R.N. Mohapatra, *Unification and Supersymmetry* (Springer, New York, 1986).
- [4] R. Casalbuoni, S. de Curtis, D. Dominici, and R. Gatto, Phys. Lett. **B155**, 95 (1985); Nucl. Phys. **B282**, 235 (1987); Nucl. Phys. **B310**, 181 (1988).
- [5] For a review of composite vector bosons see B. Schrempp, Proceedings of the 23rd International Conference on High Energy Physics, Berkeley (World Scientific, Singapore 1987); see also U. Baur *et al.*, Phys. Rev. **D35**, 297 (1987); M. Kuroda *et al.*, Nucl. Phys. **B261**, 432 (1985).

- [6] J.L. Hewett and T.G. Rizzo, Phys. Rep. **183**, 193 (1989).
- [7] J.L. Hewett, *Proceedings of the Workshop on Physics and Experiments with Linear  $e^+e^-$  Colliders*, F.A. Harris, S.L. Olsen, S. Pakvasa, and X. Tata, eds. April 26-30, 1993, Waikoloa, Hawaii (World Scientific, Singapore, 1993)p. 246.
- [8] M. Cvetič, F del Aguila and P. Langacker, *Proceedings of the Workshop on Physics and Experiments with Linear  $e^+e^-$  Colliders*, F.A. Harris, S.L. Olsen, S. Pakvasa, and X. Tata, eds., April 26-30, 1993, Waikoloa, Hawaii (World Scientific, Singapore, 1993)p. 929.
- [9] F. del Aguila, Proceedings of the XVII International School of Theoretical Physics “Standard Model and Beyond ’93”, Szczyrk, (1992), Acta Physica Polonica **B25**, 1317 (1994) ([hep-ph/9404323](#)).
- [10] D. Chang, R. Mohapatra, and M. Parida, Phys. Rev. **D30**, 1052 (1984).
- [11] E. Ma, Phys. Rev. **D36**, 274 (1987); K.S. Babu *et al.*, Phys. Rev. **D36**, 878 (1987); J.F. Gunion *et al.* Int. J. Mod. Phys. **A2**, 118 (1987); T. G. Rizzo, Phys. Lett. **B206** 133 (1988).
- [12] H. Georgi, E. Jenkins, and E.H. Simmons, Phys. Rev. Lett. **62** 2789 (1989); *ibid* **63**, 1540 (1989)**E** ; Nucl. Phys. **B331**, 541 (1990); V. Barger and T.G. Rizzo, Phys. Rev. **D41** 956 (1990).
- [13] A very small sampling of other models with  $Z'$ 's is: R. Foot and O. Hernández, Phys. Rev. **D41**, 946 (1990); R. Foot, O. Hernández, and T.G. Rizzo, Phys. Lett. **B246**, 183 (1990); A. Bagnoid, T.K. Kuo, and N. Nakagawa, Int. J. Mod. Phys. **A2** 1327 (1987); **2**, 1351 (1987); K.T. Mahanthappa and P.K. Mohapatra, Phys. Rev. **D42**, 1732 (1990); **42**, 2400 (1990); X. Li and E. Ma, Phys. Rev. Lett. **47**,1788 (1981); Phys. Rev. **D46**, 1905 (1992); X.-G. He *et al.*, Phys. Rev. **D44**, 2118 (1991).
- [14] P. Langacker and M. Luo, Phys. Rev. **D45**, 278 (1992).
- [15] L.S. Durkin and P. Langacker, Phys. Lett **B166**, 436 (1986); Amaldi *et al.*, Phys. Rev. **D36**, 1385 (1987); G. Altarelli *et al.*, Phys. Lett **B245**, 669 (1990); Nucl. Phys. **B342**, 15 (1990); Phys. Lett. **B261**, 146 (1991); *ibidem* **B263**, 459 (1991); F.M. Renard and C. Verzegnassi, Phys. Lett. **217**, 199 (1989); *ibidem* **225**, 431 (1989); *ibidem* **260**, 225 (1991); F. del Aguila, W. Hollik, J.M. Moreno, and M. Quiros, Phys. Rev. **D40**, 2481 (1989); F. del Aguila, J.M. Moreno, and M. Quiros, Nucl. Phys., **B361**, 45 (1991); Phys. Lett. **B254**, 479 (1991); Nucl. Phys., **B372**, 3 (1992); T.G. Rizzo, Phys. Rev. **D40**, 3035 (1989); *Proceedings of the 1990 Summer Study on High Energy Physics*. ed

- E. Berger, June 25-July 13, 1990, Snowmass Colorado (World Scientific, Singapore, 1992) p. 233; V. Barger, J.L. Hewett and T.G. Rizzo, Phys. Rev. **D42**, 152 (1990); J.L. Hewett, Phys. Lett. **B238**, 98 (1990); M.C. Gonzalez-Garcia and J.W. F. Valle, Nucl. Phys. **B345**, 312 (1990); Phys. Lett. **B236** 360 (1990); *ibidem* **259**, 365 (1991); A. Djouadi *et al.*, Nucl. Phys. **B349**, 48 (1991); G. Altarelli, R. Barbieri, and S. Jadach, Nucl. Phys. **B369**, 3 (1992); F. del Aguila, M. Cvetič, F. del Aguila, and P. Langacker, in the Proceedings of the Workshop on *Physics and Experiments at Linear  $e^+e^-$  Colliders*, Waikoloa, Hawaii, April 26-30, 1993, World Scientific 1993 (F. Harris et al. eds.), p. 490.
- [16] For a recent analysis, see P. Langacker, `hep-ph # 9412361`, to be published in *Precision Tests of the Standard Electroweak Model*, ed. P. Langacker (World Scientific, Singapore 1995).
- [17] Particle Data Group, Phys. Rev. **D50**, 1173 (1994).
- [18] CDF Collaboration, Abe *et al.*, FERMILAB-PUB-94-198-E (July, 1994).
- [19] R.S. Chivukula, E.H. Simmons, and J. Terning, BUUEP-94-37 (December, 1994), `hep-ph/9412309`.
- [20] P. Langacker, R. Robinett, and J. Rosner, Phys. Rev. **D30**, 1470 (1984).
- [21] F. del'Aguila, J.M. Morena, and M. Quiros, Phys. Rev. **D40**, 2481 (1989); T.G. Rizzo, Phys. Rev. **D48**, 4705 (1993); J.L. Rosner, Phys. Rev. **D35**, 2244 (1987); V. Barger *et al.*, Phys. Rev. **D35**, 2893 (1987); F. del'Aguila, M. Quiros, and F. Zwirner, Nucl. Phys. **B287**, 419 (1987); V. Barger, N.G. Deshpande, and K. Whisnant, Phys. Rev. **D35**, 1005 (1987); P. Chiappetta *et al.*, Proceedings of the Large Hadron Collider Workshop, ed. G. Jarlskog and D. Rein, CERN Report 90-10 (1990) p. 686.
- [22] S. Capstick and S. Godfrey, Phys. Rev. **D37**, 2466 (1988).
- [23] S. Godfrey, Phys. Rev. **D51**, 1402 (1995) (`hep-ph/9411237`).
- [24] J.L. Hewett and T.G. Rizzo, *Proceedings of the 1990 Summer Study on High Energy Physics*, ed E. Berger, June 25-July 13, 1990, Snowmass Colorado (World Scientific, Singapore, 1992) p. 222.
- [25] E. Eichten, I. Hinchliffe, K.D. Lane, and C. Quigg, Rev. Mod. Phys. **56**, 579 (1984).
- [26] J. Kubar-André and F.E. Paige, Phys. Rev. **D19**, 221 (1979); G. Altarelli, R.K. Ellis, and G. Martinelli, Nucl. Phys. **B143**, 521 (1978); **B146**, 544 (1978).



- [27] J.L. Hewett and T.G. Rizzo, Phys. Rev. **D45**, 161 (1992).
- [28] P. Langacker and U. Sankar, Phys. Rev. **D40**, 1569 (1989).
- [29] T. Rizzo, SLAC-PUB-6719 (November 1994), hep-ph/9411326.
- [30] G. Belanger and S. Godfrey, Phys. Rev. **D34**, 1309 (1986); **D35**, 378 (1987); F. Boudjema, B.W. Lynn, F.M. Renard, C. Verzegnassi, Z. Phys. **C48**, 595 (1990); A. Blondel, F.M. Renard, P. Taxil, and C. Verzegnassi, Nucl. Phys. **B331**, 293 (1990); P.J. Franzini and F.J. Gilman, Phys. Rev. **D35**, 855 (1987); M. Cvetič and B. Lynn, Phys. Rev. **D35**, 1 (1987); B.W. Lynn and C. Verzegnassi, Phys. Rev. **D35**, 3326 (1987); T.G. Rizzo *ibid.*, **36**, 2699(1987); A. Bagneid, T.K. Kuo, and G.T. Park *ibid.*, **44**, 2188 (1991); A. Djouadi, A. Leike, T. Riemann, D. Schaile and C. Verzegnassi, Z. Phys. **C56** 289 (1992); A. Leike, Z. Phys. **C62**, 265 (1994); J.L. Hewett and T.G. Rizzo, *Proceedings of Physics and Experiments with Linear Colliders*, ed. R. Orava *et al.*, Saariselkä, Finland (World Scientific, 1992) Vol II p. 489; T.G. Rizzo, *ibid.*
- [31] These systematic errors are based on simulations of an SLD type detector operating at a 500 GeV  $e^+e^-$  collider. T. Barklow, private communication.
- [32] S. Capstick and S. Godfrey, Phys. Rev. **D35**, 3351 (1987).
- [33] V.D. Angelopoulos *et al.*, Phys. Lett. **176B** 203 (1986); F. Cornet and R. Rückl, Phys. Lett. **184** 263 (1987); F. Cornet and H.-U. Martyn, Proceedings of the Large Hadron Collider Workshop, ed. G. Jarlskog and D. Rein, CERN Report 90-10 (1990) p. 986.
- [34] F. del Aguila, M. Cvetič, and P. Langacker, Phys. Rev. **D48**, R969 (1993).
- [35] F. del Aguila, M. Quirós, and F. Zwirner, Nucl. Phys. B **284**, 530 (1987); P. Kalyniak and M. Sundaresan, Phys. Rev. D **35**, 75 (1987).
- [36] M. Cvetič, P. Langacker, and B. Kayser, Phys. Rev. Lett. **68**, 2871 (1992).
- [37] N. Deshpande, J. Gunion, and F. Zwirner, in the *Proceedings of the Workshop on Experiments Detectors and Experimental Areas for the Supercollider* (Berkeley 1987); N. Deshpande, J. Grifols, and A. Méndez, Phys. Lett. **B208**, 141 (1988).
- [38] F. del Aguila, L. Ametller, R. Field, and L. Garrido, Phys. Lett. **B201**, 375 (1988); Phys. Lett. **B221**, 408 (1989).
- [39] M. Cvetič and P. Langacker, Phys. Rev. **D42**, 1797 (1990).
- [40] M. J. Duncan and P. Langacker, Nucl. Phys. **B277**, 285 (1986).

- [41] F. del Aguila and J. Vidal, *Int. J. of Math. Phys.* **A4**, 4097 (1989).
- [42] M. Cvetič and P. Langacker, *Phys. Rev.* **D 46**, R14 (1992).
- [43] J. Anderson, M. Austern, and B. Cahn, *Phys. Rev. Lett.* **69**, 25 (1992) and *Phys. Rev.* **D46**, 290 (1992).
- [44] A. Fiandrino and P. Taxil, *Phys. Rev.* **D44**, 3490 (1991); *Phys. Lett.* **B292**, 242 (1992).
- [45] F. del Aguila, B. Alles, L. Ametller and A. Grau, *Phys. Rev.* **D48**, 425 (1993).
- [46] J. Hewett and T. Rizzo, *Phys. Rev.* **D47**, 4981 (1993).
- [47] M. Cvetič and P. Langacker, *Phys. Rev.* **D46**, 4943 (1992).
- [48] T. Rizzo, *Phys. Rev.* **D47**, 956 (1993).
- [49] A. Henriques and L. Poggioli, ATLAS Collaboration, Note PHYS-NO-010 (October 1992);
- [50] T.G. Rizzo, *Phys. Rev.* **D48**, 4236 (1993).
- [51] P. Mohapatra, *Mod. Phys. Lett.* **A8**, 771 (1993).
- [52] T. Rizzo, *Phys. Lett.* **B192**, 125 (1987); J.L. Hewett and T.G. Rizzo, *Phys. Rev.* **D45**, 161 (1992).
- [53] J. Hewett and T. Rizzo, ANL-HEP-CP-93-51 (August 1993).
- [54] P. Langacker and M. Luo, *Phys. Rev.* **D44**, 817 (1991).
- [55] M. Cvetič, P. Langacker and J. Liu, *Phys. Rev.* **49**, 2405 (1994).
- [56] A. Djouadi, A. Leike, T. Riemann, D. Schaile and C. Verzegnassi, *Z. Phys.* **C56** (1992) 289.
- [57] J. Hewett and T. Rizzo, in the Proceedings of the *Workshop on Physics and Experiments with Linear  $e^+e^-$  Colliders*, September 1991, Saariselkä, Finland, R. Orava ed., Vol. II, p. 489; *ibidem* p. 501.
- [58] F. del Aguila and M. Cvetič, *Phys. Rev.* **D50**, 3158 (1994).
- [59] A. Leike, *Z. Phys.* **C62** (1994) 265; see also D. Choudhury, F. Cuypers, and A. Leike, *Phys. Lett.* **B333** (1994) 531.
- [60] F. del Aguila, M. Cvetič and P. Langacker, UG-FT-45/94, UPR-636-T (January, 1995), [hep-ph/9501390](http://hep-ph/9501390).
- [61] LEP Collaborations, CERN preprint, CERN/PPE/93-157 (August 1993).